

# Standing spin-wave mode structure and linewidth in partially disordered perpendicularly magnetized sub-micron Permalloy disc arrays

N. Ross,<sup>1, a)</sup> M. Kostylev,<sup>1, b)</sup> and R. L. Stamps<sup>1</sup>

*School of Physics, University of Western Australia, Crawley, WA, Australia*

(Dated: 1 June 2019)

Standing spin wave mode frequencies and linewidths in partially disordered perpendicularly magnetized arrays of sub-micron Permalloy discs are measured using vector network analyzer ferromagnetic resonance. Fitted demagnetizing parameters decrease with increasing array disorder. Frequency separation between first and second radial modes is found to be higher than theoretical predictions for isolated discs. The relative frequencies between successive spin wave modes are unaffected by changes to the long-range array ordering. An increase in standing spin wave broadening at low applied magnetic fields that has a magnitude which is correlated to array disorder is observed. The fitted intrinsic damping parameter is found to increase with increasing array disorder.

Keywords: ferromagnetic-resonance, perpendicular, sub-micron-disc

## I. INTRODUCTION

Understanding the high-frequency dynamics of sub-micron diameter, nanometer thickness magnetic discs is important for applications in data storage<sup>1–5</sup> and spintronics<sup>6,7</sup> technologies. There have been a number of recent studies concerned with spin wave mode structure<sup>8–18</sup> and linewidths<sup>19–23</sup> in the in-plane magnetized configuration for such dipole coupled arrays. There have also been experimental studies conducted for disc arrays in the perpendicularly magnetized state, with characterization achieved by cavity ferromagnetic resonance<sup>24,25</sup> (cavity FMR) and magnetic resonance force microscopy<sup>26</sup> (MRFM). The mode structure in the perpendicularly magnetized geometry can be modelled more easily than in the tangentially magnetized case, because of the cylindrical symmetry of the disc in the axial direction.

In the cited studies of perpendicularly magnetized arrays the measured spin wave spectra matched well with theoretical predictions, but due to the experimental techniques used this comparison could only take place over limited frequency ranges. In addition, only in one of the studies was there an investigation into the effect of array packing on the FMR mode structure. In Ref. 24, variation of the pitch along one direction of the square array was found to affect the absolute field positions of the peaks in the spectrum, but not the relative field positions of individual peaks. Additionally, none of the studies cited deal with the effect of array packing density on the FMR linewidth in the perpendicularly magnetized geometry.

In this study, Vector Network Analyzer FMR (VNA-FMR) was used to study the perpendicularly magnetized spin wave mode structure and linewidth of a series of four

disc array samples with varying degrees of array ordering, over a wide range of excitation frequencies. These arrays have been previously studied in the tangentially magnetized state, and details of their production and characterization can be found in Ref. 22. Each of the four array samples consisted of a locally trigonal array of Permalloy discs, with each array distinguished from the others by a different degree of long-range ordering. The long-range ordering was quantified with a parameter  $\phi'$ , the average amount of variation in the lattice angle in degrees per millimeter.

## II. EXPERIMENT

Film	d [nm]	$\phi'$ [° mm <sup>-1</sup> ]	$4\pi M_S$ [kOe]
f3c	-	-	8.49
f3b	695 ± 28	6.0 ± 0.8	-
f3a	703 ± 37	9.4 ± 1.1	-
f2c	-	-	8.69
f2a	697 ± 31	11.3 ± 1.7	-
f1c	-	-	8.85
f1a	699 ± 28	19.9 ± 2.1	-

TABLE I. Table showing average disc diameter,  $d$ , array variation per unit length  $\phi'$ , and saturation magnetization  $4\pi M_S$  for the samples used in this study. All discs had thickness  $27 \pm 3$  nm.

The structural characteristics of each of the samples are listed in Table I. Samples f3c, f2c, and f1c were continuous film sections cut from the parent film from which f3a and f3b, f2a, and f1a, respectively, were patterned. The samples were placed face-down on an 8 mil microstrip waveguide connected to a two-port vector network analyzer and magnetized out-of-plane with respect to the substrate. The VNA-FMR measurement was performed at frequencies between 6 and 17 GHz, in intervals

<sup>a)</sup> Electronic mail: rossn2282@gmail.com

<sup>b)</sup> Electronic mail: kostylev@cyllene.uwa.edu.au

of one GHz. The microwave transmission parameter  $S_{21}$  was measured as the applied magnetic field was swept through the experimentally available range, in analogy to the cavity FMR experiment. Negligible reflections allowed  $S_{11}$  to be ignored.<sup>27</sup> An example of the spin wave spectra obtained is shown in Figure 1. This spectrum of modes is in qualitative agreement with those measured previously,<sup>24–26</sup> and as will be seen in the next section arises directly from the cylindrical symmetry of the discs in the axially magnetized configuration.

Previous investigation of these array samples<sup>22</sup> showed no evidence of significant material or structural differences between the four samples. Specifically, atomic force microscopy images showed that all four samples had smooth disc boundaries, and there was no significant evidence in the SQUID-measured in-plane hysteresis loops of structures which do not support compensated magnetic vortices at remanence. With the exception of small differences in saturation magnetizations  $M_S$  and parent film linewidths  $\Delta H$ , the only parameter known to vary significantly between the arrays was the degree of array ordering,  $\phi'$ .

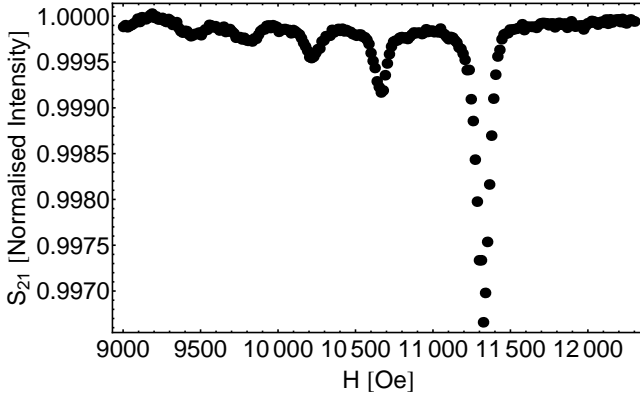


FIG. 1. Plot of normalized transmission parameter  $S_{21}$  vs applied out-of-plane magnetic field  $H$  for sample f2a, at an excitation frequency of 10 GHz, as measured by VNA-FMR. Five radial modes are resolved.

### III. THEORY OF MODE STRUCTURE IN PERPENDICULARLY MAGNETIZED DISCS

The theory for FMR modes in isolated, perpendicularly magnetized discs presented here was first applied to sub-micron discs in Ref. 24, and is based on the dipole-exchange theory of spin wave spectra in unrestricted in-plane magnetic films<sup>28,29</sup> and a method of the calculation of demagnetising fields in nonellipsoidal bodies.<sup>30</sup> This model does not take into account the interaction between elements in a closely packed array and therefore does not take into account the effects of disorder in that array. Such effects are expected to manifest in experiment as deviations from the predictions made with this model.

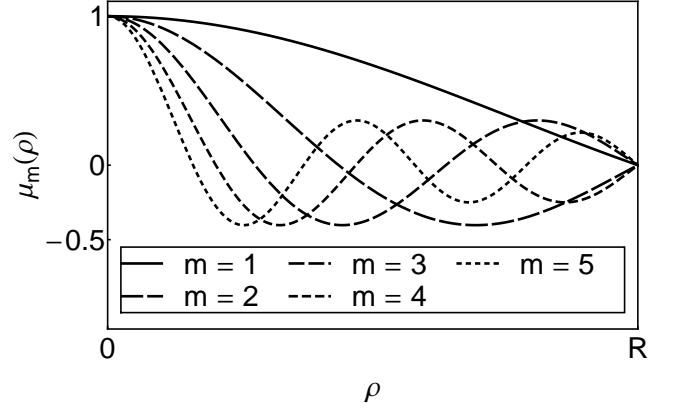


FIG. 2. Plot of the theoretical spin wave eigenmodes  $\mu_m(\rho)$  for the first five modes for a perfect, isolated disc.

In this theory, the finite radius  $R$  of the disc is considered to allow only discrete values of the in-plane wave vector:  $k \rightarrow k_m$ ,  $m = 1, 2, 3, \dots$ . The nonellipsoidal geometry of the disc means that the demagnetising field inside the dot is inhomogeneous, with the internal bias field becoming a function of the disc radius  $\rho$ . The strong dipolar pinning at the disc edges produces dipolar eigenmodes with zeroth-order Bessel function profiles:

$$\mu_m(\rho) = J_0(k_m \rho) \quad (1)$$

The standing mode profiles of the first five modes of such a disc geometry are shown in Figure 2. These profiles have been confirmed experimentally by Mewes *et al.* in square arrays of sub-micron diameter discs using MRFM.<sup>26</sup> These modes profiles correspond in principle to the peaks in Figure 1, with the largest amplitude, highest-field peak the  $m = 1$  mode. Assuming that there is no significant out-of-plane film anisotropy, the frequencies of these modes are:

$$\begin{aligned} \omega_m^2 = & \gamma^2 \left( H - 4\pi M_S N_m + \frac{2Ak_m^2}{M_S} \right) \\ & \times \left( H - 4\pi M_S N_m + \frac{2Ak_m^2}{M_S} + 4\pi M_S \left( 1 - \frac{1 - e^{-k_m L}}{k_m L} \right) \right), \end{aligned} \quad (2)$$

for  $\gamma$  the gyromagnetic ratio;  $H$  the applied magnetic field;  $M_S$  the saturation magnetization;  $A$  the exchange stiffness constant; and  $L$  the disc thickness.  $N_m$  is determined as in Ref. 31:

$$N_m = \frac{1}{A_m} \int_0^R N(\rho) J_0(k_m \rho)^2 \rho d\rho, \quad (3)$$

with:

$$A_m = \frac{R^2 J_1(k_m R)^2}{2}, \quad (4)$$

and the radius-dependent demagnetising factor averaged

over the thickness:<sup>30</sup>

$$N(\rho) = -\frac{R}{L} \int_0^\infty J_0(t\rho) J_1(tR) \frac{e^{-Lt} - 1}{t} dt. \quad (5)$$

This term converges when integrated up to a sufficiently large value of  $t$ . In the case of the calculations to follow,  $t = 10^7$  was used.

## IV. RESULTS

### A. FMR mode structure

The range of applied magnetic fields available for the field sweep was defined at its lower end by the minimum field expected to be necessary to saturate the magnetization of the discs out of the substrate film plane,  $H \simeq 4\pi M_S$ , and at its upper end by the maximum field attainable with the available electromagnet,  $H = 14$  kOe. A representative plot of the resonance frequencies  $f$  of the first five radial modes against the resonance field  $H_{res}$  in this field range is shown in Figure 3. Points missing from the plots have been excluded because the associated peaks were too small or too broad for the centre frequency to be determined. The solid lines are the fits for the data to Equation 2, having left  $N_m$  as the free fitting parameter in each case.

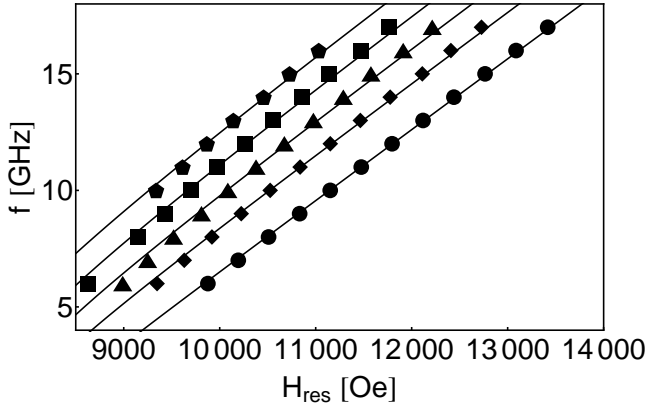


FIG. 3. Plot of frequency  $f$  vs out-of-plane magnetic resonance field  $H_{res}$  for the first five radial modes of sample f3b (circles:  $m = 1$ ; diamonds:  $m = 2$ ; triangles:  $m = 3$ ; squares:  $m = 4$ ; pentagons:  $m = 5$ ), as measured by VNA-FMR. Solid lines are fits to Equation 2. This data is representative of those data obtained from all of the samples.

The fitted values of  $N_m$  are shown in Figure 4, plotted against  $\phi'$ , the parameter characterizing the array ordering. The values are tabulated in Table II, along with the values of  $N_m$  calculated for a theoretical isolated ‘disc’, 700 nm diameter, 27 nm thickness. The uncertainties in the  $N_m$  values were calculated by propagating the uncertainties in the disc radius  $R$  and thickness  $L$  through

Film	$N_1 \times 10$	$N_2 \times 10$	$N_3 \times 10$	$N_4 \times 10$	$N_5 \times 10$
‘disc’	9.51	9.40	9.35	9.33	9.31
f3b	$9.67 \pm 0.05$	$9.44 \pm 0.08$	$9.38 \pm 0.10$	$9.37 \pm 0.12$	$9.39 \pm 0.15$
f3a	$9.69 \pm 0.08$	$9.43 \pm 0.14$	$9.37 \pm 0.18$	$9.32 \pm 0.21$	$9.37 \pm 0.23$
f2a	$9.65 \pm 0.04$	$9.38 \pm 0.08$	$9.32 \pm 0.10$	$9.28 \pm 0.12$	$9.34 \pm 0.14$
f1a	$9.49 \pm 0.04$	$9.21 \pm 0.08$	$9.12 \pm 0.10$	$9.08 \pm 0.12$	$9.07 \pm 0.14$

TABLE II. Table of demagnetising factors  $N_m$  as calculated from Equation 3 for a disc of 700 nm diameter, 27 nm thickness (denoted ‘disc’), and for disc array samples f3b, f3a, f2a, and f1a, as extracted by fitting equation 2 to the data in Figure 3.

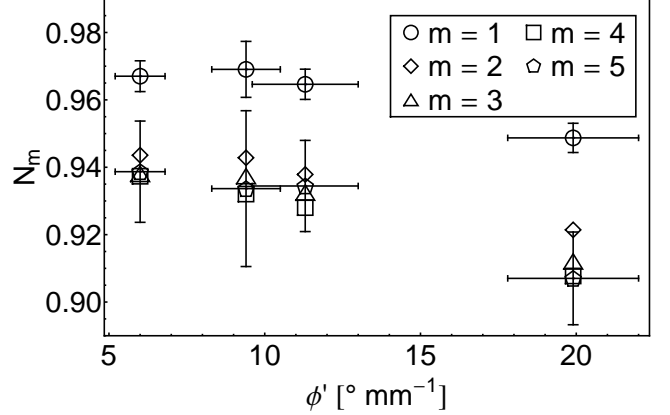


FIG. 4. Plot of the first five demagnetising factors  $N_m$  vs lattice angle variation parameter  $\phi'$  for the first five radial modes, as extracted from fits to the VNA-FMR data shown in Figure 3. Error bars are included only on the  $m = 1$  and  $m = 5$  modes for clarity; errors for the other modes have magnitudes which vary between these minimum and maximum values respectively.

the fit. These uncertainties likely represent slight overestimates, as much of the uncertainty in the film thickness was the result of finite measurement precision, rather than film-to-film thickness variation. The curiosity that  $N_m$  values for f1a appear to be smaller than for the isolated ‘disc’ can be explained by postulating a small systematic underestimate of all three  $M_S$  values, associated with calibration of the applied magnetic field strength. The ‘real’  $N_m$  values are probably consistently slightly higher than those quoted in the table, but relative values are unaffected.

There was a slight decrease in demagnetising parameter  $N_m$  with increasing array disorder. In the absence of unknown structural differences between arrays, this might be attributable to a reduction in average dipole coupling strength due to lowered symmetry and/or a slight reduction in neighbour density associated with increased array disorder. While changes to  $N_m$  across the range of  $\phi'$  available were small enough to be comparable to the uncertainties,  $N_m$  values for an isolated disc differ from the value  $N = 1$  for a continuous film by less

than 0.07, as can be seen in Table II. The change in  $N_m$  with reduced array ordering cannot be expected be higher than this difference value. That the change was almost half this value for a given mode is actually an indication that the loss of ordering actually causes dramatic relative changes in the demagnetising fields of the array.

In addition to changes with  $\phi'$ , there was a dramatic difference in demagnetising factors between those extracted from fits to experimental data and those calculated for an isolated disc. Displayed across the  $\phi'$  range of all four samples was the phenomenon that the difference between  $N_1$  and the higher order demagnetising factors  $N_{2,3,4,5}$  was larger than for the isolated disc. That is, the first radial mode appeared to possess a demagnetising field that was significantly more like that of a continuous film in character than the higher order modes.

This departure from the theory for an isolated disc may give useful information about the character of the dipole coupling in the arrays. The structural uniformity of the discs means that all but very small differences in edge character can be ruled out as causes of this effect. All of the radial modes are assumed to be the result of the same out-of-plane static magnetization configuration, effectively ruling out static dipole effects as the cause of this difference in demagnetising factors. On the other hand, the dynamic dipole field of the first radial mode can be expected to be stronger than for the other modes, since it alone has no nodes across the diameter of the disc. The difference between  $N_1$  and  $N_{2,3,4,5}$  might therefore be interpreted as being contributed to by dynamic dipole coupling between elements of the array.

Film	$\overline{f_2 - f_1}$	$\overline{f_3 - f_2}$	$\overline{f_4 - f_3}$	$\overline{f_5 - f_4}$
'disc'	1.59	1.42	1.42	1.48
f3b	$1.93 \pm 0.09$	$1.44 \pm 0.06$	$1.36 \pm 0.05$	$1.40 \pm 0.08$
f3a	$2.00 \pm 0.17$	$1.44 \pm 0.09$	$1.49 \pm 0.09$	$1.39 \pm 0.07$
f2a	$2.01 \pm 0.09$	$1.44 \pm 0.06$	$1.47 \pm 0.06$	$1.26 \pm 0.04$
f1a	$2.03 \pm 0.09$	$1.55 \pm 0.06$	$1.47 \pm 0.06$	$1.46 \pm 0.05$

TABLE III. Table of average frequency differences in GHz between fits to Equation 2 of successive modes, on the field interval [10000-12000] Oe for a disc of 700 nm diameter, 27 nm thickness (denoted 'disc'), with saturation magnetization  $M_S$  and spectroscopic splitting factor  $g$  identical to film f3c, and for disc array samples f3b, f3a, f2a, and f1a.

The large accessible frequency range afforded by VNA-FMR meant that the frequency difference between successive modes could be measured over a wide range of resonance fields. The frequency difference between modes was calculated by averaging the frequency separation between fits to the data for successive modes over a field

interval  $[H_{\min}, H_{\max}]$ :

$$\overline{f_{m+1} - f_m} = \frac{1}{H_{\max} - H_{\min}} \int_{H_{\min}}^{H_{\max}} \frac{\omega_{m+1} - \omega_m}{2\pi} dH. \quad (6)$$

Rather than calculation of the frequency difference between the experimentally measured data themselves, this approach was adopted because the different resonance fields  $H_{\text{res}}$  of successive modes were not the same due to the particular manner in which the VNA-FMR experiment was accomplished. The frequency differences between successive experimentally measured modes are tabulated in Table III alongside the same for the theoretical isolated 'disc'.

The frequency difference for the first two modes,  $f_2 - f_1$ , is larger in all cases than for the theoretical, isolated 'disc'. This is consistent with the difference in fitted first and higher order radial mode demagnetising factors already mentioned. In the absence of undetected disc geometry differences between array samples, it might likewise be interpreted as a manifestation of dynamic dipole coupling of first radial modes in the arrays.

This phenomenon was observable because of the large range of excitation frequencies and magnetic fields over which a resonance could be observed in this study, a consequence of the samples being large enough to be measured using VNA-FMR. Kakazei *et al.* observed no such frequency difference in their study of nickel discs in a square array,<sup>24</sup> perhaps as a result of either the lack of frequency range experimentally available in their cavity FMR study or due to the reduced magnetization of nickel and its consequent lower coupling strength. The difference in local symmetry between the square and trigonal arrays may also have contributed to this discrepancy. However, the results of the study presented here were in accord with this previous study's findings with regard to there being a change in frequencies of all modes, but no observable change in the relative frequencies between those modes with reduction in array density. Within the limits of experimental uncertainty, increasing  $\phi'$  changed the absolute frequencies of all modes, but not the relative frequencies between modes.

## B. FMR linewidth

The very small amplitudes of modes beyond the second radial mode and the small magnetic background signal precluded the extraction of meaningful linewidths from these modes. Given that the previously detailed measurements of mode structure revealed the second and higher order modes behaving similarly, this limited data set is likely representative of the behavior of all the modes. Plots of the field linewidths  $\Delta H$  extracted from Lorentzian fits to the first two radial modes of all four samples are shown in Figure 5, alongside the linewidth data from the corresponding parent continuous films.

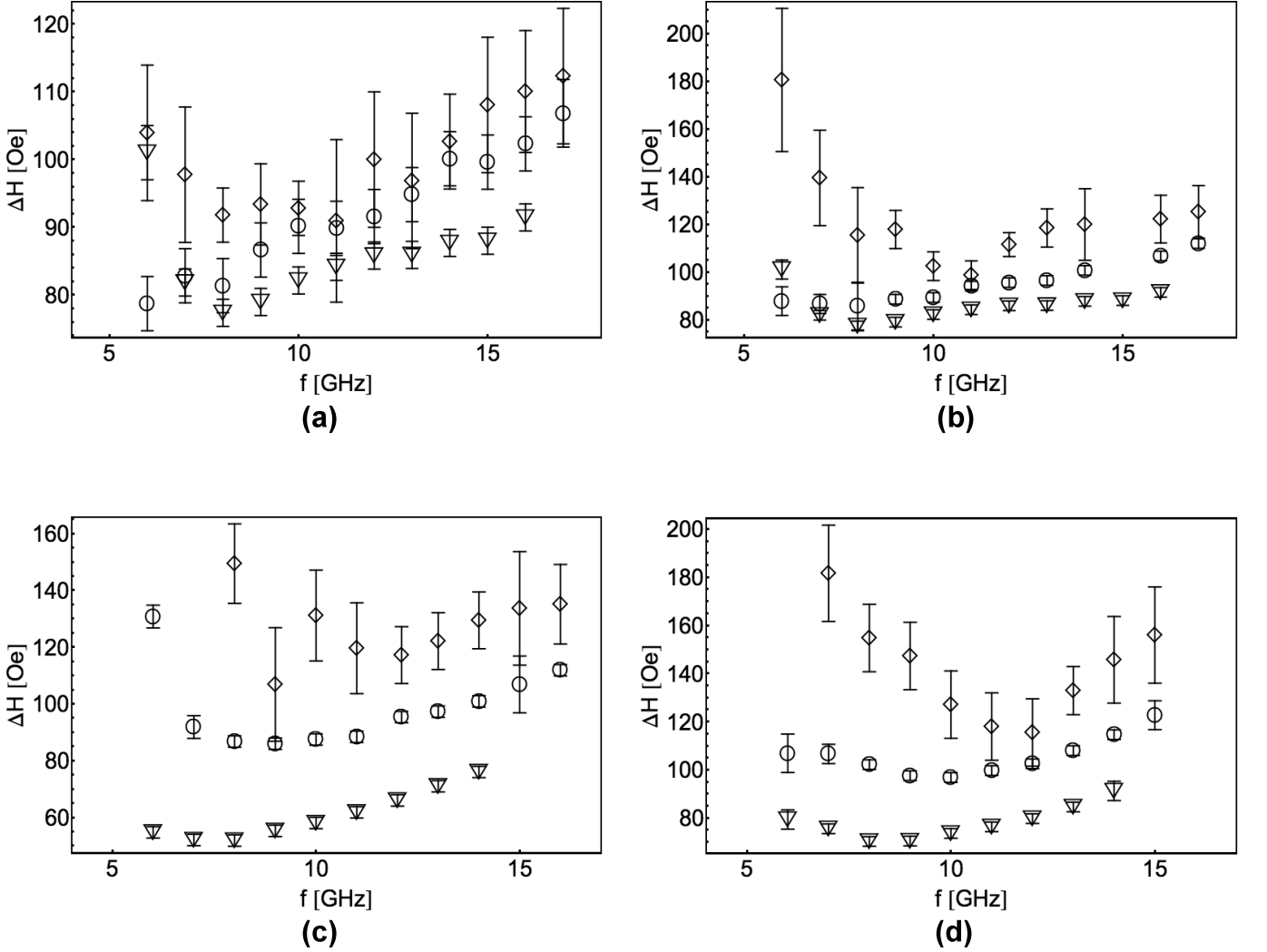


FIG. 5. Plot of FMR linewidth  $\Delta H$  vs frequency  $f$  for samples (a) f3b, (b) f3a, (c) f2a, (d) f1a, for applied field in the direction of the film perpendicular, as measured by VNA-FMR. The first (circles) and second (diamonds) radial modes are shown alongside the data from the corresponding parent continuous films (inverted triangles).

In previous studies of spin wave mode broadening in thin films<sup>32</sup> and patterned structures,<sup>20,22</sup> the effects of intrinsic and extrinsic damping have been separated by fitting the data with the equation:

$$\Delta H = \Delta H_0 + \frac{4\pi\alpha}{\gamma\mu_0} f, \quad (\text{SI}) \quad (7)$$

where  $\alpha$  is the intrinsic damping parameter in the Landau-Lifshitz-Gilbert equation,<sup>33,34</sup> the ‘viscous’ damping of energy to the lattice,<sup>35</sup> and  $\Delta H_0$  is a term representing inhomogeneous broadening. However,  $\Delta H$  does not increase with frequency in the affine fashion expected from Equation 7, even in the case of the parent continuous films. Instead, at low frequency values the linewidths are very broad, decreasing to some minimum, then increasing with increasing frequency in an approxi-

mately linear fashion from some onset frequency,  $f_{\text{cut-off}}$ , or equivalently from the resonance field at this frequency.

It can be seen from Figure 5 that the broadening of the linewidth below the cut-off frequency or field is more extreme for the second radial mode than for the first, and that the broadening is more extreme for more disordered films. Given that the perpendicular magnetized state is an unstable equilibrium, it can be conjectured that this phenomenon may be related to static dipole coupling between elements. Close to the field required to saturate the discs perpendicularly, disorder might be expected to change the local out-of-plane demagnetizing field, leading to a spreading of magnetization directions and resonance frequencies across the array. Arrays with more disorder could be expected to experience a greater range of local resonance fields, and thus exhibit a greater

linewidth broadening due to this effect. The similarity of the individual discs between arrays already mentioned makes it unlikely that the linewidth differences observed were due to local effects, such as disc edge roughness.

The data in Figure 5 were fit with Equation 7, but only after all data points below the apparent frequency of onset of linearity  $f_{\text{cut-off}}$  were removed. The fit parameters for the parent continuous films, and for the first and second radial modes are tabulated in Tables IV, V and VI, respectively. The data is presented in three separate tables to highlight that the differing mode structures may preclude useful direct comparison of fit values between modes, or between parent and patterned films. There was an apparent increase in the fitted intrinsic damping parameter  $\alpha_m$  in the first and second radial modes with respect to the fundamental mode of the parent continuous films. Plots of intrinsic damping parameter  $\alpha$  against array ordering parameter  $\phi'$  are shown in Figure 6 for both the first and second modes.

Film	$f_{\text{cut-off}}$ [GHz]	$\alpha_1 \times 10^3$	$\Delta H_0$ [Oe]
f3c	8	$2.43 \pm 0.39$	$65.3 \pm 3.2$
f2c	8	$6.05 \pm 0.57$	$18.9 \pm 4.2$
flc	9	$5.57 \pm 0.87$	$36.5 \pm 6.5$

TABLE IV. Table showing fit data for each sample to Equation 7 for the fundamental modes of the parent continuous film samples. The fits for each sample are made excluding data from frequencies below  $f = f_{\text{cut-off}}$ .

Film	$f_{\text{cut-off}}$ [GHz]	$\alpha_1 \times 10^3$	$\Delta H_0$ [Oe]
f3b	6	$3.65 \pm 0.53$	$64.3 \pm 4.1$
f3a	8	$4.32 \pm 0.40$	$61.6 \pm 3.5$
f2a	10	$5.65 \pm 0.51$	$49.9 \pm 4.2$
fla	10	$6.89 \pm 0.91$	$49.8 \pm 7.3$

TABLE V. Table showing fit data for each sample to Equation 7 for the first radial mode. The fits for each sample are made excluding data from frequencies below  $f = f_{\text{cut-off}}$ .

Film	$f_{\text{cut-off}}$ [GHz]	$\alpha_2 \times 10^3$	$\Delta H_0$ [Oe]
f3b	11	$5.07 \pm 2.97$	$56.1 \pm 28.0$
f3a	11	$6.24 \pm 2.49$	$59.0 \pm 21.2$
f2a	12	$7.50 \pm 6.10$	$58.1 \pm 54.8$
fla	12	$20.69 \pm 11.37$	$-46.2 \pm 98.9$

TABLE VI. Table showing fit data for each sample to Equation 7 for the second radial mode. The fits for each sample are made excluding data from frequencies below  $f = f_{\text{cut-off}}$ .

For the same arrays magnetized in the plane of the substrate, the intrinsic damping parameter  $\alpha$  extracted

from Equation 7 has been observed to be slightly higher for patterned films than for unpatterned films, but uncorrelated to array ordering.<sup>22</sup> It is not clear whether the assumption that the inhomogeneous damping  $\Delta H_0$  is independent of field and frequency holds in such patterned systems, that is, it is not clear that Equation 7 holds. If it does not, then the fitted value of  $\alpha$  and the real value of the intrinsic damping parameter may be different. Furthermore, it must be acknowledged that the uncertainties accompanying the linear increases in Figure 6 are large, especially for the second radial mode. The value of  $\alpha$  in the patterned films appears to be unrelated to the value from the parent continuous films, perhaps because of the differing mode structures. However, no convincing explanation as to why  $\alpha$  should increase with increasing array disorder can be conjectured at this time.

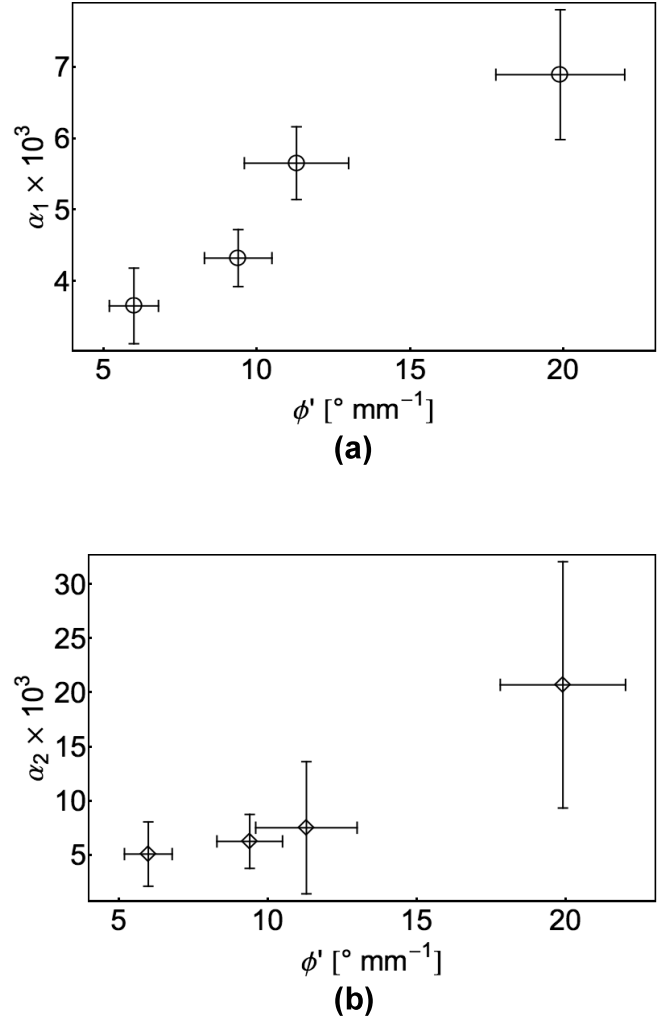


FIG. 6. Plot of intrinsic damping parameter  $\alpha$  against array ordering parameter  $\phi'$  for the (a) first and (b) second radial modes.

## V. CONCLUSIONS

The standing spin wave mode structure and linewidth broadening in a series of trigonal sub-micron diameter disc arrays in the perpendicularly magnetized state was investigated using vector network analyzer ferromagnetic resonance. Comparison to theory of measurements over a wide range of frequencies allowed deviations of the mode structure from that of an isolated disc to be identified. These deviations revealed the importance of array ordering to the absolute size of the magnetizing factors. Deviations from expected frequency differences between modes suggested that the standing spin wave modes were influenced by dynamic dipole coupling between discs. The relative values of demagnetizing fields for successive modes were essentially unaffected by changes to the array symmetry, and the relative mode structure was consequently unaffected by increasing disorder in the the arrays.

Anomalously large linewidth broadenings were observed close to the out-of-plane demagnetizing fields of the arrays, and conjectured to be caused by differing local magnetization directions due to dipole coupling between disordered discs. At sufficiently high applied fields, the linewidth increased linearly with excitation frequency, with a gradient that increased with increasing array disorder. The physical origins of these changes to the as-fitted intrinsic damping parameter in both this perpendicularly magnetized geometry and those already reported for the tangentially magnetized geometry<sup>22</sup> remain unknown. It is thus unclear whether these phenomena are related.

There appears to be a common conclusion from the ferromagnetic resonance studies of the close-packed trigonal disc arrays in both magnetization geometries: that linewidth is affected by the lack of preservation of the long-range symmetry of the array, but resonance frequency is not. Since it is known that increasing the diameter-to-pitch ratio of a square array of discs affects the in-plane magnetized resonance field,<sup>8</sup> this in turn suggests that the changes in ferromagnetic linewidth resonance observed in this study were the product of changes in the array symmetry itself, rather than of the slightly lower packing fractions that come as a consequence of that reduction in symmetry.

## ACKNOWLEDGEMENTS

This work was supported in part by the Australian Research Council under Discovery Grant “Magnetic nanostructures for emerging technologies”. N. Ross is supported by a University of Western Australia Hackett Postgraduate Scholarship.

- <sup>2</sup>Thomson T, Hu G and Terris B D 2006 *Phys. Rev. Lett.* **96** 257204
- <sup>3</sup>Shaw J M, Rippard W H, Russek S E, Reith T and Falco C M 2007 *J. Appl. Phys.* **101** 023909
- <sup>4</sup>Hellwig O, Berger A, Thomson T, Dobisz E, Bandic Z Z, Yang H, Kercher D S and Fullerton E E 2007 *Appl. Phys. Lett.* **90** 162516
- <sup>5</sup>Shaw J M, Russek S E, Thomson T, Donahue M J, Terris B D, Hellwig O, Dobisz E and Schneider M L 2008 *Phys. Rev. B* **78** 024414
- <sup>6</sup>Kiselev S I, Sankey J C, Krivorotov I N, Emley N C, Schoelkopf R J, Buhrman R A and Ralph D C 2003 *Nature* **425** 380
- <sup>7</sup>Deac A M, Fukushima A, Kubota H, Maehara H, Suzuki Y, Yuasa S, Nagamine Y, Tsunekawa K, Djayaprawira D D and Watanabe N 2008 *Nat. Phys.* **4** 803
- <sup>8</sup>Jorzick J, Demokritov S O, Hillebrands B, Bartenlian B, Chappert C, Decnanini D, Rousseaux F and Cambril E 1999 *Appl. Phys. Lett.* **75** 3859
- <sup>9</sup>Guslienko K Y and Slavin A N 2000 *J. Appl. Phys.* **87** 6337
- <sup>10</sup>Jung S, Watkins B, De Long L, Ketterson J B and Chandrasekhar V 2002 *Phys. Rev. B* **66** 132401
- <sup>11</sup>Jung S, Ketterson J B and Chandrasekhar V 2002 *Phys. Rev. B* **66** 132405
- <sup>12</sup>Politi P and Pini M 2002 *Phys. Rev. B* **66** 214414
- <sup>13</sup>Rivkin K, Heifetz A, Seivert P R and Ketterson J B 2004 *Phys. Rev. B* **70** 184410
- <sup>14</sup>Gubbiotti G, Madami M, Tacchi S, Carlotti G and Okuno T 2006 *J. Appl. Phys.* **99** 08C701
- <sup>15</sup>Giovannini L, Montoncello F and Nizzoli F 2007 *Phys. Rev. B* **75** 024416
- <sup>16</sup>Rivkin K, Saslow W, De Long L E and Ketterson J B 2007 *Phys. Rev. B* **75** 174408
- <sup>17</sup>Rivkin K, Xu W, De Long L E, Metlushko V V, Ilic B and Ketterson J B 2007 *J. Magn. Magn. Mater.* **309** 317
- <sup>18</sup>Nevirkovets I P, Chernyashevskyy O, Ketterson J B, Metlushko V and Sarma B K 2008 *J. Appl. Phys.* **104** 063920
- <sup>19</sup>Schneider M L, Shaw J M, Kos A B, Gerrits T, Silva T J and McMichael R D 2007 *J. Appl. Phys.* **102** 103909
- <sup>20</sup>Shaw J M, Silva T J, Schneider M L and McMichael R D 2009 *Phys. Rev. B* **79** 184404
- <sup>21</sup>Rivkin K, Nevirkovets I P, Chernyashevskyy O, Ketterson J B, Sarma B K and Metlushko V 2009 *J. Magn. Magn. Mater.* **321** 3324
- <sup>22</sup>Ross N, Kostylev M and Stamps R L 2010 *arXiv* **1005** 0452v2
- <sup>23</sup>Kakazei G N, Mewes T, Wigen P E, Hammel P C, Slavin A N, Pogorelov Y G, Costa M D, Golub V O, Guslienko K Y and Novosad V 2008 *J. Nanosci. Nanotechnol.* **8** 2811
- <sup>24</sup>Kakazei G N, Wigen P E, Guslienko K Y, Novosad V, Slavin A N, Golub V O, Lesnik N A and Otani Y 2004 *Appl. Phys. Lett.* **85** 443
- <sup>25</sup>Kostylev M, Magaraggia R, Ogrin F Y, Sirotkin E, Mescheryakov V F, Ross N and Stamps R L 2008 *IEEE Trans. Mag.* **44** 2741
- <sup>26</sup>Mewes T, Kim J, Pelekov D V, Kakazei G N, Wigen P E, Batra S and Hammel P C 2006 *Phys. Rev. B* **74** 144424
- <sup>27</sup>Counil G, Crozat P, Devolder T, Chappert C, Zoll S and Fournel R 2004 *IEEE Trans. Mag.* **42** 3321
- <sup>28</sup>Kalinkos B A and Slavin A N 1986 *J. Phys. C* **19** 7013
- <sup>29</sup>Kalinkos B A, Kostylev M P, Kozhus N V and Slavin A N 1990 *Journal of Physics: Condensed Matter* **2** 1990
- <sup>30</sup>Joseph R I and E S 1965 *J. Appl. Phys.* **36** 1579
- <sup>31</sup>Guslienko K Y, Chantrell R W and Slavin A N 2003 *Phys. Rev. B* **68** 024422
- <sup>32</sup>Kalarickal S S, Krivosik P, Wu M, Patton C E, Schneider M L, Kabos P, Silva T J and Nibarger J P 2006 *J. Appl. Phys.* **99** 093909
- <sup>33</sup>Landau L and Lifshitz E 1935 *Phys. Z. Sowjetunion* **8** 153
- <sup>34</sup>Gilbert T L 1956 Ph.D. thesis Illinois Institute of Technology
- <sup>35</sup>Lenz K, Wende H, Kuch W, Baberschke K, Nagy K and Jánossy A 2006 *Phys. Rev. B* **73** 144424

<sup>1</sup>Terris B D and Thomson T 2005 *J. Phys. D* **38** R199